

Impact of cross linking chain of N,N'-bis(naphthalen-|-y|)-N,N'-bis(phenyl)-benzidine on temperature dependent transport properties

M. Ramar^{1,2}, S. S. Rawat¹, R. Srivastava², S. K. Dhawan^{1,2}, C. K. Suman^{2*}

¹Academy of Scientific and Innovative Research (AcSIR), CSIR-National Physical Laboratory Campus, Dr. K. S. Krishnan Road, New Delhi-110012, India

²CSIR-Network of Institutes for Solar Energy, CSIR-National Physical Laboratory, Dr. K. S. Krishnan Road, New Delhi-110012, India

*Corresponding author. E-mail: sumanck@nplindia.org

Received: 16 November 2015, Revised: 24 February 2016 and Accepted: 01 June 2016

ABSTRACT

The impact of cross linking chain of N, N'-bis (naphthalen-|-y|)-N, N'-bis(phenyl)-benzidine (NPB) was studied for optoelectrical properties having focus on temperature dependent transport properties. The Spiro structured NPB compound is closed in itself and the thin film surface roughness is less in comparison to NTNPB compounds. Both absorptions and photoluminescence shows a shift of 10 nm towards higher wavelength in case of cross linked spiro structured compound. The mobility calculated in SCLC region for NT and Spiro NPB was 1.32×10^{-7} and $3.3 \times 10^{-7} \text{ cm}^2 \text{ V}^{-1} \text{ s}^{-1}$, respectively. Both the compounds show single relaxations and can be modeled as an RC equivalent circuits. The dc conductivity for both the compounds was explained by Mott's VRH models showing 3D transport mechanism. The hopping distance for NT and Spiro NPB compounds is 0.8 and 0.5 nm, respectively. The hopping conduction process can be explained clearly using correlated barrier hopping model. The cross linking of the compounds shows two orders of less density of states. Copyright © 2016 VBRI Press.

Keywords: Cross linking; thin film; impedance; hopping; mott's temperature; conductivity.

Introduction

The attraction of organic semiconductors for researchers is due to possibilities of manufacturing of optoelectronic devices for lighting application, photovoltaics applications and electronics applications. All these devices can be fabricated at low-cost, large area and light weight [1–5]. The performance of organic semiconductor devices is influenced by the morphology of the corresponding materials and the morphology of the organic semiconductor materials depends on the glass transition temperature. The simple way of tuning the materials glass transition temperature is by changing the structure of the compound with closed and open structure. The high glass transition temperature of material is achieved by introducing the concept of cross linking or simply converting them into Spiro. There are many different materials viz electron transport material; hole transport material; anode/cathode buffer layers and light emissive layers used for optoelectronic devices [6–10]. The concept of spiro or crosslinking is possible for any organic semiconductors. Now a days; the Spiro small molecules organic compounds are getting attention due to its application in dye sensitized solar cells and Perovskite based organic solar cells [11,12]. The interface between organic semiconductors and metals or organic – organic compound is also dependent on the glass transition temperature or simple the morphology of the corresponding thin film. The carrier injection or

transport in the device depends on appropriate organic semiconductor surface morphology. The main contribution of organic semiconductors morphology is reduction of the contact resistance between organic semiconductors and metal. At the same time; the interface energy barrier is reduced because of band bending phenomena. These contributions support to improve the device life time [13,14]. The well-known and studied hole transport organic materials are N,N'-bis(naphthalen-|-y|)-N,N'-bis(phenyl)-benzidine (NPB) which is in two structural forms non-crosslinked (NT-NPB) and crosslinked (spiro-NPB) [15]. The electrical and optical properties of these organic materials have been extensively investigated earlier but the electrical properties comparison of NT and spiro organic semiconductors needs more research focus because the cross linking of the benzenes leads to the fused nature of the molecules. The fused nature of molecules influences π - π interaction, rigidity and planarity. Hence comparison of electrical properties for non-fused and fused nature of the organic molecules will be helpful for designing the organic electronic devices like transistors and organic light emitting transistors.

In this paper; we have presented the temperature dependent electrical properties of NT-NPB and spiro-NPB hole only device using Atomic force microscopy, absorption and photo-luminescence (PL), current-voltage characteristics and broad frequency range (100Hz - 1MHz) impedance spectroscopy.

Experimental

The indium tin oxide (ITO) coated glass substrates was used to fabricate hole only device (HOD) in the structure of ITO/organic material (NT or Spiro NPB)/Au to explore the carrier dynamics of the materials. The organic semiconductor films and the gold (Au) thicknesses were maintained at 120 nm and 100 nm, respectively. The ITO patterned glass substrates were cleaned ultrasonically with soap solution, de-ionized (DI) water and organic solvents acetone and isopropyl alcohol. The substrate was dried at 120 °C for 30 minutes into vacuum chamber. The thermal deposition of organic semiconductors and metal layers were performed in a high vacuum deposition system using shadow masks. The base pressure of the chamber was maintained at $\sim 10^{-6}$ Torr. The deposition rate for organic layers and metal electrode were maintained at 1-2 Å/s and 2-5 Å/s, respectively. The overlap area of ITO and gold electrode are the device area, which is 9 mm².

The optical properties of organic semiconductors thin film were measured using PL setup (Horiba) and UV-Viz Spectrometer. The electrical properties were evaluated using Impedance spectroscopy (IS) by Impedance/Gain-Phase Analyzer (Solartron, model SI 1260) System. The device impedance as a function of AC frequency and DC bias was measured by superimposing a 100 mV amplitude AC signal with DC bias voltages.

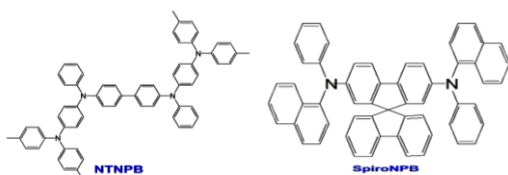


Fig. 1. Chemical structure of NTNPB and SpiroNPB.

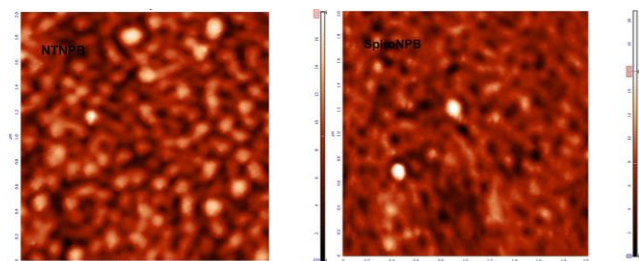


Fig. 2. AFM images of NTNPB and SpiroNPB thin film deposited in silicon substrate.

Results and discussion

The molecular structure of NTNPB and SpiroNPB are shown in Fig. 1. The chain is open in the NT structure of NPB whereas the chains are cross linked in the spiro structure of NPB. Simply the spiro structure are closed in itself hence are less reactive to the environment. Fig. 2 shows the atomic force microscopy (AFM) images of NT and spiro NPB thin film deposited on silicon substrate. All AFM images were captured in the tapping mode of operation using AFM system (NT-MDT Solver Pro). The RMS value of surface roughness for NT and spiro NPB thin film are 2.51 nm and 1.78 nm, respectively.

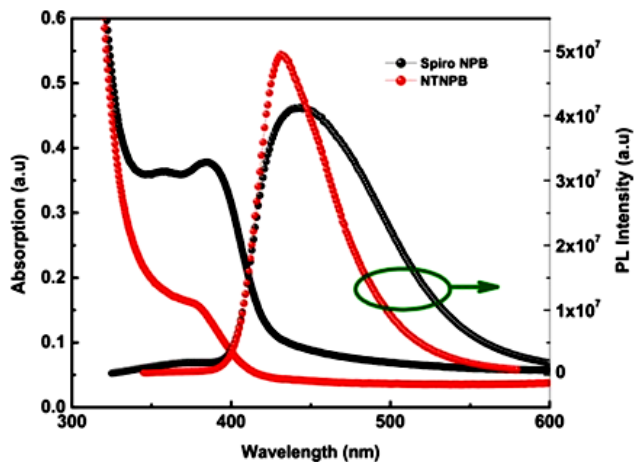


Fig. 3 Absorption spectra and Photoluminescence (PL) Intensity spectra of NTNPB and SpiroNPB 50 nm thin films on glass substrate.

The almost smooth images of thin film indicate the uniform deposition of both the materials. However, the surface roughness of spiro NPB decreases compares to NTNPB this may be due to closed cross linked chain of the materials. Fig. 3 shows the spectra of absorption and PL for 200 to 1000 nm wavelength. The maximum absorption for NTNPB and spiroNPB thin films was found at a wavelength of ~ 380 nm and 390 nm, respectively. There is a shift in the peak of the spiro NPB of ~ 10 nm wavelength towards higher wavelength. The photo-luminescence intensity (PL) peak for NT and Spiro NPB thin film was observed at ~ 440 nm and 450 nm. Again an increase of 10 nm wavelength in maximum of PL spectra was observed.

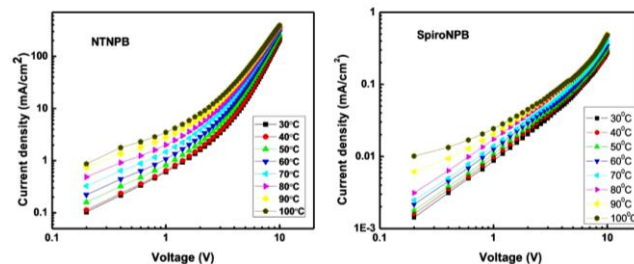


Fig. 4. Current density – Voltage (J - V) characteristics of ITO|NT or SpiroNPB|Au with temperature variation.

Fig. 4 shows the current density voltage (J - V) characteristics of hole only NTNPB and SpiroNPB devices. The current densities (J) for both devices have a linear increase with voltage in low region and at high bias voltage region; the current density has non-linear increases. At low voltages (first region of J - V curve), the Log J - V plots shows nearly unity slope, while at higher voltages, the slope is about 2 or more. Hence the conductivity is visibly Ohmic at low voltage region and for higher voltages region it is space charge limited conductivity ($SCLC$). The Ohmic region current density can be represented as [16]

$$J = qn_0\mu \frac{v}{d}, \quad (1)$$

where, n_0 , μ and d are the concentration of thermally activated carriers, mobility and thickness of the organic semiconductor ($d = 120$ nm). In the ohmic region; current

for both compound increases with increase of temperature too. Similar trend of current increase is observed in high voltage region. At high voltages region (second region of J-V curve) $J \propto V^2$, the current is limited by space charges with a single discrete set of shallow traps. The SCLC current density is

$$J = \frac{9}{8} \epsilon \mu \theta \frac{V^2}{d^3}, \quad (2)$$

where, μ is the charge carrier mobility, θ is the trapping fraction and ϵ is the organic semiconductor dielectric constant (taken as 3.5). The trapping fraction can be

$$\theta = \frac{n_o}{n_o + n_t}$$

where, n_o is the free charge carrier density and n_t is the trapped charge carrier density. The hole mobility of NT and Spiro NPB calculated assuming trap free SCLC ($n_t = 0$) was 1.32×10^{-7} and $3.3 \times 10^{-7} \text{ cm}^2 \text{ V}^{-1} \text{ s}^{-1}$, respectively which is comparable to the mobility obtained by OTFT [17]. Almost same order of mobility was found for both the compounds.

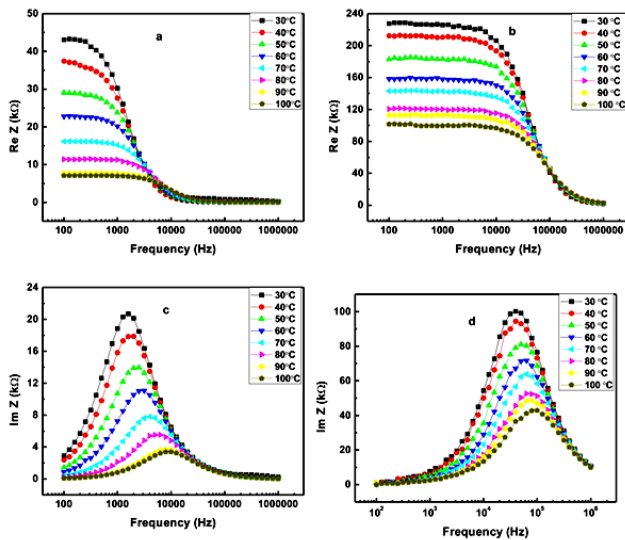


Fig. 5. (a, b) Real part of impedance as a function of frequency at various applied bias voltages for NTNPB and SpiroNPB (c, d) Imaginary part of impedance as a function of frequency at different temperatures for NTNPB and Spiro NPB.

Fig. 5 Shows the frequency dependent variation of real (Re Z) and imaginary (Im Z) parts of impedance at different temperature. The complex impedance $Z(f)$ as a function of frequency can be represented as,

$$Z(f) = Z'(f) + Z''(f) \quad (3)$$

The real and imaginary parts of impedance are denoted as Z' and Z'' , respectively. For NT NPB device the real Z is constant upto a frequency of 1 kHz and for Spiro NPB device it is constant upto 500 kHz frequency. In high frequency region; the ReZ for NT and Spiro NPB device had decreasing trends from 1 kHz to 10 kHz and from 500 kHz to 900 kHz, respectively. The Re Z magnitude decreases with increase of temperature at low frequency but

the Re Z magnitude value merges for higher frequency at all studied temperature.

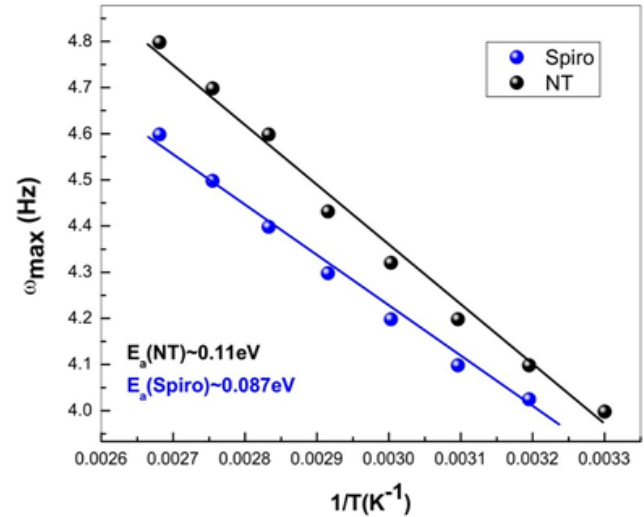


Fig. 6. Variation of relaxation frequency (ω_{max}) with $1/T$.

Both NT and Spiro NPB hole only device show an increase in ac conductivity with frequency and a single relaxation process. A maxima peak $\text{Im}(Z)_{max}$ was observed in $\text{Im}Z$ curve for all studied temperature range. The frequency corresponding to $\text{Im}(Z)_{max}$ called relaxation frequency. The relaxation frequency shows a shift to higher values of frequency with increase of temperature which corresponds to temperature dependent loss in the materials.

The relaxation process at the peak is defined by the condition,

$$\omega_m \tau_m = 1 \quad (4)$$

where, τ_m is the relaxation time. The relaxation frequency was observed to be shifted towards higher side of the frequency by increase of temperature, this shifts corresponds to lowering value of relaxation time. The variation of relaxation frequency with temperature is shown in **Fig. 6**. For hopping conduction; the relaxation frequency is given by [18]

$$\omega_m = \omega_0 \exp(-E_a / K_B T), \quad (5)$$

where, ω_0 and E_a are the phonon frequency (usually in the range of 10^{12} - 10^{13} Hz) and activation energy, respectively. The estimated activation energy for NT and Spiro NPB are 0.11 and 0.087 eV, respectively. The plots of Cole-Cole for both NT and Spiro NPB at different temperatures are shown in **Fig. 7**. A single semicircle is observed at all studied temperature range and the semicircle size decreases rapidly as the temperature increases. The electrical model corresponding to Cole-Cole plot of both devices are an RC equivalent electrical circuit in which contact series resistance R_S are in parallel to a single resistance (R_p) and the capacitance (C_p) network. The R_S is the electrode contact resistance which is the minimum values of Re Z and it is about 60Ω for all devices. The values of R_S at different temperature are nearly same. The maximum value of Re Z corresponds to the summing up of R_S and R_p .

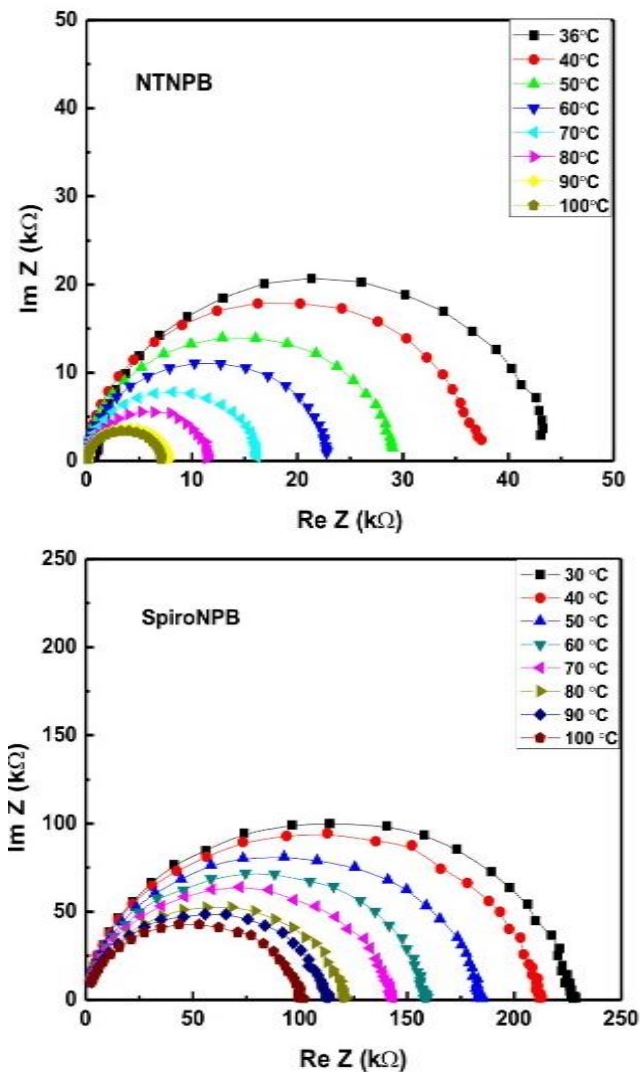


Fig. 7. Cole-Cole plots of NTNPB and Spiro NPB hole only device at different temperature.

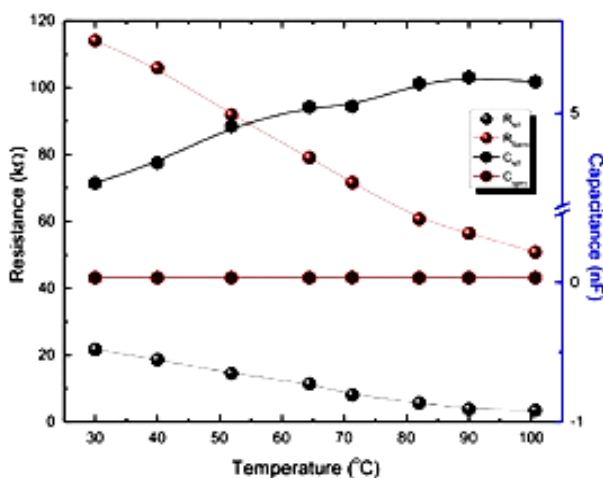


Fig. 8. The variation of bulk resistance RP and capacitance CP with temperature.

The variation of resistance and capacitance with temperature are shown in Fig. 8. It can be seen that the R_p for both NT and spiro NPB decreases as the temperature

increases whereas C_p for NTNPB increases with increase of temperature but for spiroNPB it is almost independent on the temperature. Generally, the intrinsic property of materials is directly related to C_p . The large number of injected carriers causes a decrease of R_p with temperature. This decrease indicates that the organic material effective conductivity will increase with the temperature. The R_p and C_p value at room temperature for NT and SpiroNPB are $\sim 20\text{k}\Omega$, $110\text{ k}\Omega$ and 4 , 0.5 nF , respectively.

The basic ac electrical conductivity equations are given by,

$$\sigma_{ac} = \frac{l}{AZf} \tag{6}$$

where, A and l are taken as the area and thickness of the device. Z represents impedance of device.

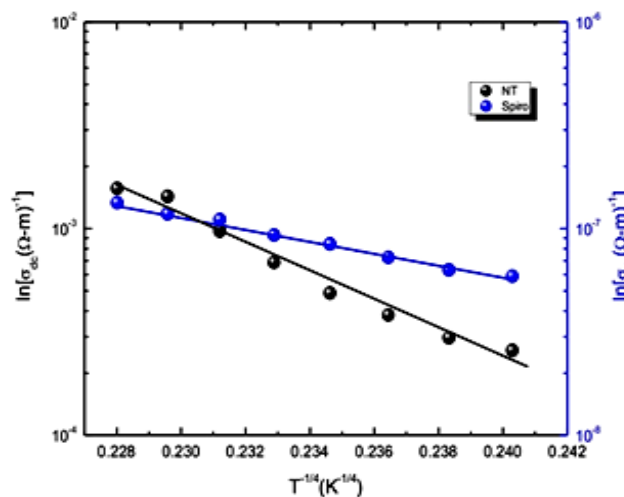


Fig. 9. Variation of dc conductivity (σ_{dc}) with $1/T^{1/4}$

Fig. 9 shows the variation of σ_{ac} with frequency at different temperature. There are two different regions of ac conductivity for studied temperature range; at low frequency it is frequency independent and at high frequency it is frequency dependent. It is clear that the frequency independent conductivity increases with temperature whereas the frequency dependent has the opposite characteristics. The onset (switch from frequency-independent to frequency-dependent region) shows a shift to higher side with temperature. The frequency dependent σ_{ac} region display a power law dependence like conducting materials given by Jonscher [19]

$$\sigma_{ac} = \sigma_{dc} + A\omega^s \tag{7}$$

where, σ_{dc} is the frequency-independent conductivity, ω is the angular frequency of the applied AC electric field in the frequency sensitive region, A and s ($0 \leq s \leq 1$) are material and doping dependent constants. According to Mott's VRH model [20], variation of dc conductivity with temperature are presented by

$$\sigma_{dc} = \sigma'_0 \exp\left[-\left(\frac{T_{MOTT}}{T}\right)^{1/4}\right] \tag{8}$$

where, σ_0 is the conductivity at infinite temperature, γ is the VRH exponent, and T_{Mott} is the Mott's characteristics temperature given by,

$$T_{Mott} = \frac{24}{[\pi K_B L_{loc}^3 N(E_f)]} \quad (9)$$

Here, L_{loc} is the localization length and $N(E_f)$ is the density of states at the Fermi level. The Mott's characteristics temperature depends on the hopping barrier. The VRH exponent (γ) is related to the dimensionality "d" by,

$$\gamma = (1/1+d) \quad (10)$$

From this equation, we may say that $\gamma = 1/4, 1/3, 1/2$ corresponds to 3, 2, and 1 dimensional system, respectively.

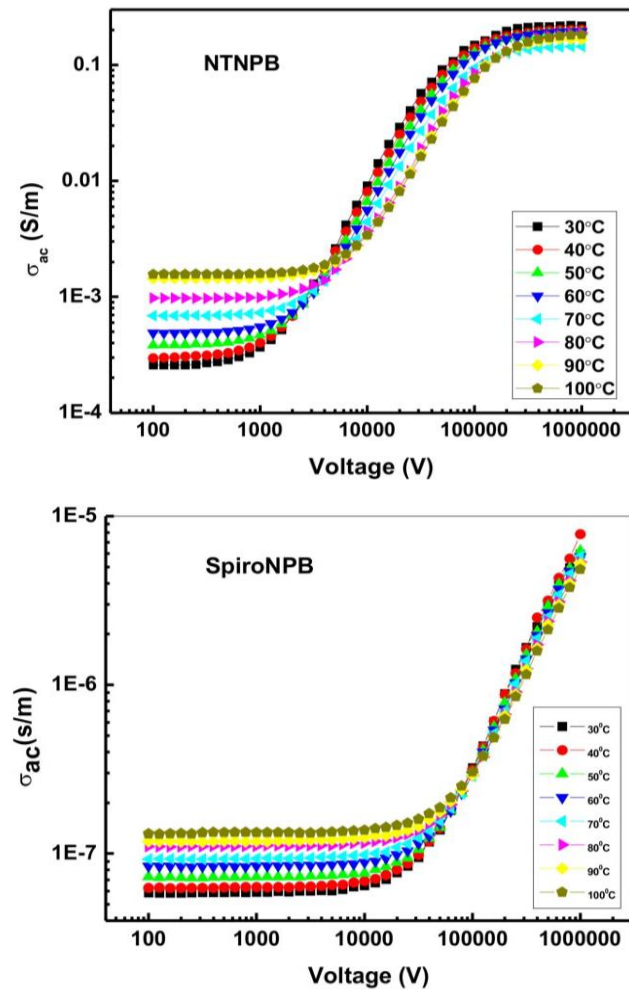


Fig. 10. The ac conductivity (σ_{ac}) variation with frequency at different temperatures.

The variations of $\ln\sigma_{ac}$ with $T^{1/4}$ are shown in Fig. 10. The experimental data are fitted nearly a straight line that indicates 3D charge transport mechanism may be the dominant charge transport mechanism. The value of T_{Mott} for NT and Spiro NPB are found to be 0.23K and 3.38 K, respectively. The correlations of conduction mechanism with frequency exponent "s" have been proposed by different theoretical models to explain the nature of

frequency and temperature dependent ac conductivity (σ_{ac}). Fig. 11 shows the variation of frequency exponents (S) with temperature. For both the compound NT and Spiro NPB the value of s is around one and decreases with increase of temperature. The main proposed theoretical models for ac conduction in amorphous semiconductors are correlated barrier hopping (CBH), classical hopping over barrier (HOB) and quantum mechanical tunneling (QMT). In QMT model; the carrier tunnels between two localized states near the Fermi level. Similarly; there is hopping of two electrons or holes simultaneously over the potential barrier between two charged defect states (bipolaron hopping) in CBH model.

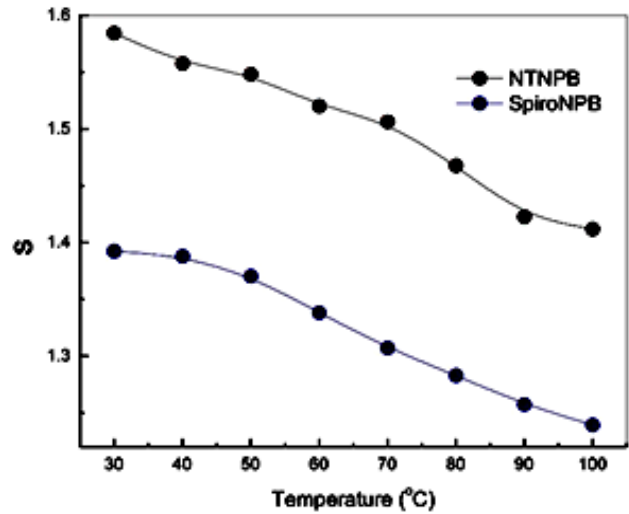


Fig. 11. The variation of exponent "s" with temperature.

The correlations of barrier height (W) with the intersite separation(R) are driven by Coulombic interaction. Barrier height (W) is presented by

$$W = W_M - \frac{n e^2}{\pi \epsilon \epsilon_0 R} \quad (11)$$

where, W_M , e , ϵ and ϵ_0 are maximum barrier height, electronic charge, dielectric constants of material and free space, respectively. The number of electrons involved in the hoping process is n; which are taken as n=1 for single polaron hopping and n = 2 for bipolaron hopping.

The ac conductivity for this mechanism are represented as [21],

$$\left. \begin{aligned} \sigma_{ac} &= \frac{n\pi^3}{24} N^2 \epsilon \epsilon_0 R \omega^6 \\ R_\omega &= \frac{n e^2}{\pi \epsilon \epsilon_0 [W_M + K T \ln(\omega \tau_0)]} \end{aligned} \right\} \quad (12)$$

where, R_ω and N are considered as the hopping distance at a frequency ω and the concentration of pair states.

In CBH model; the frequency exponent can be assessed as,

$$S = 1 - \frac{6KT}{W_M + KT \ln(\omega \tau_0)} \quad (13)$$

In Fig. 12(a), the calculated minimum hopping distance, the binding energy (W_M) and (b) density of states $N(E_F)$ for both NT and spiro NPB compound are shown. The binding energy for both the compound increases with temperature and there is similar trend in density of states whereas the hopping distance has completely opposite trend. The hopping distance decreases with temperature. The room temperature binding energy for NT NPB ($\sim 0.4\text{eV}$) is less in comparison to spiro NPB ($\sim 0.25\text{eV}$). Similar trend is observed for hopping distance viz R_w for NT NPB $\sim 0.8\text{nm}$ and for Spiro NPB $\sim 0.55\text{ nm}$.

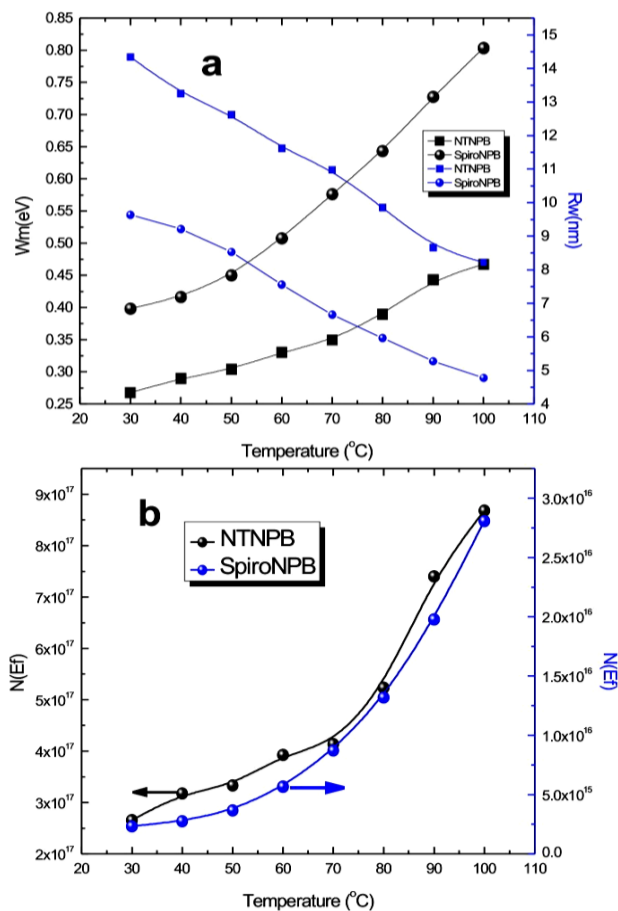


Fig. 12. (a) Temperature dependence of minimum hopping distance (R_{\min}), binding energy (W_{\min}) and (b) density of states (N_{E_F}) at 1kHz for NTNPB and SpiroNPB.

At Fermi level (for 100 kHz); the value of calculated density of states (DOS) for both the materials NT and Spiro NPB are 2.5×10^{17} and $4 \times 10^{15} \text{eV}^{-1} \text{cm}^{-3}$, respectively. The dominating factor for DOS near the Fermi level are impurities, doping, decomposition or the different molecular phases and the interfacial region [22]. The deep tails of the intrinsic Gaussian DOS distribution may be broaden because of the Coulombic interaction of the charge carriers released and the dopant or interfacial region [23]. Hence the cross linking of organic structures leads to decrease of the total density of states.

Conclusion

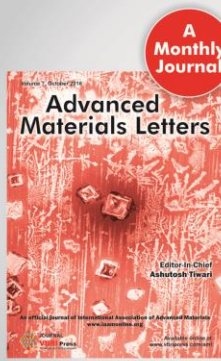
Two structures of NPB were studied; the NTNPB structure has open chain whereas the spiroNPB structure is closed in

itself that's makes spiroNPB compound environmentally stable. The surface roughness of the spiroNPB compound thin film is low in comparison to NTNPB compound thin film. The absorption and photoluminescence of spiroNPB compound shifts 10nm towards higher wavelengths. The hole mobility in the SCLC region of both the compound are of the same order ($\sim 10^{-7} \text{cm}^2 \text{V}^{-1} \text{S}^{-1}$). Both the compounds show single relaxation process and the ac conductivity increases with frequency. The activation energy for NT and Spiro NPB are 0.11 and 0.087 eV respectively. The model of R-C equivalent electrical circuits can be well fitted with the Cole-Cole plot of both the compounds. The dc conductivity was fitted to Mott's VRH model and Mott's temperature for both compounds is almost near room temperature $\sim 0.23\text{ K}$ for NTNPB and 3.3K for SpiroNPB. The carriers transport in both the compound is 3D transport. The ac conductivity is well fitted with correlated barrier hopping model. The hopping distance for NT and Spiro NPB compounds is 0.8 and 0.5 nm, respectively. The DOS at Fermi levels for NT and Spiro NPB are of the order of 10^{17} and 10^{15} , respectively. The cross linking of the compounds shows two orders of less density of states. The electrical and optical properties studied above can make a way to designing the fused and nonfused organic compound for improvement of device performance. The transistor based light emitting devices are being under optimization in our laboratory based on these compounds.

References

- Tang, C. W.; VanSlyke, S. A; *Appl. Phys. Lett.*, **1987**, *51*, 913. DOI: [10.1063/1.98799](https://doi.org/10.1063/1.98799)
- Forrest, S. R; *Nature*, **2004**, *428*, 911. DOI: [10.1038/nature02498](https://doi.org/10.1038/nature02498)
- Ramar, M.; Suman, C. K.; Manimozhi, R.; Ahamad, R.; Srivastava, R.; *RSC Adv.*, **2014**, *4*, 32651. DOI: [10.1039/C4RA04966G](https://doi.org/10.1039/C4RA04966G)
- Huang, J.; Pfeiffer, M.; Werner, A.; Blochwitz, J.; Leo, K.; Liu, S.; *Appl. Phys. Lett.*, **2002**, *80*, 139. DOI: [10.1063/1.1432110](https://doi.org/10.1063/1.1432110)
- Tang, C. W.; *Appl. Phys. Lett.*, **1986**, *48*, 183. DOI: [10.1063/1.96937](https://doi.org/10.1063/1.96937)
- Kulkarni, A. P.; Tonzola, C. J.; Babel, A.; Jenekhe, S. A.; *Chem. Mater.*, **2004**, *16*, 4556. DOI: [10.1021/cm0494731](https://doi.org/10.1021/cm0494731)
- Huh, D. H.; Kim, G. W.; Kim, G. H.; Kulshreshtha, C.; and Kwon, J. H.; *Synth. Met.*, **2013**, *180*, 79. DOI: [10.1016/j.synthmet.2013.07.021](https://doi.org/10.1016/j.synthmet.2013.07.021)
- Wang, Y. L.; Ye, J. Y.; *Adv. Mater. Res.*, **2013**, *830*, 215. DOI: [10.4028/AMR.830.215](https://doi.org/10.4028/AMR.830.215)
- Park, C. H.; Lee, H. J.; Hwang, J. H.; Kim, K. N.; Shim, Y. S.; Jung, S. G.; Park, C. H.; Park, Y. W.; Ju, B. K.; *ACS Appl. Mater. Interfaces*, **2015**, *7*, 6047. DOI: [10.1021/am5091066](https://doi.org/10.1021/am5091066)
- Higuchi, T.; Nakanotani, H.; Adachi, C.; *Adv. Mater.*, **2015**, *27*, 2019. DOI: [10.1002/adma.201404967](https://doi.org/10.1002/adma.201404967)
- Dualeh, A.; Moehl, T.; Tétreault, N.; Teuscher, J.; Gao, P.; Nazeeruddin, M. K.; Grätzel, M.; *ACS Nano.*, **2014**, *8*, 362. DOI: [10.1021/nn404323g](https://doi.org/10.1021/nn404323g)
- Dualeh, A.; Moehl, T.; Nazeeruddin, M. K.; Grätzel, M.; *ACS Nano*, **2013**, *7*, 2292. DOI: [10.1021/nn4005473](https://doi.org/10.1021/nn4005473)
- Grozea, D.; Turak, A.; Yuan, Y.; Han, S.; Lu, Z. H.; Kim, W. Y.; *J. Appl. Phys.*, **2007**, *101*, 033522. DOI: [10.1063/1.2434943](https://doi.org/10.1063/1.2434943)
- Tong, K. L.; Tsang, S. W.; Tsung, K. K.; Tse, S. C.; So, S. K.; *J. Appl. Phys.*, **2007**, *102*, 093705. DOI: [10.1063/1.2804109](https://doi.org/10.1063/1.2804109)

15. Chen, H.; Gao, C. H.; Jiang, Z. Q.; Zhang, L.; Cui, L. S.; Ji, S. J.; Liao, L. S.; *Dyes Pigments*, **2014**, *107*, 15.
DOI: [10.1016/j.dyepig.2014.03.006](https://doi.org/10.1016/j.dyepig.2014.03.006)
16. Lampert, M. A.; Mark, P.; *Current Injection in Solids*, Academic, New York, **1970**.
ISBN-10: 0124353509, ISBN-13: 978-0124353503
17. Saragi, T. P. I.; Fuhrmann-Lieker, T.; Salbeck, J.; *Adv. Funct. Mater.*, **2006**, *16*, 966.
DOI: [10.1002/adfm.200500361](https://doi.org/10.1002/adfm.200500361)
18. Pollak, M.; Pike, G. E., *Phys. Rev. Lett.*, **1972**, *28*, 1449.
DOI: [10.1103/PhysRevLett.28.1449](https://doi.org/10.1103/PhysRevLett.28.1449)
19. S. R. Elliott, *Adv. Phys.*, **1987**, *36*, 135.
DOI: [10.1080/00018738700101971](https://doi.org/10.1080/00018738700101971)
20. N. F. Mott and E. A. Davis, *Electronic Processes in Non-Crystalline Materials*, Oxford University Press, Oxford, 971.
ISBN 10: 0198512597, ISBN 13: 9780198512592
21. Soosen, S. M.; Chandran, A.; Koshy, J.; George, K. C., *J. Appl. Phys.*, **2011**, *109*, 113702.
DOI: [10.1063/1.3594709](https://doi.org/10.1063/1.3594709)
22. Shen, C.; Kahn, A.; Schwartz, J., *J. Appl. Phys.*, **2001**, *89*, 449.
DOI: [10.1063/1.1333740](https://doi.org/10.1063/1.1333740)
23. Arkhipov, V. I.; Heremans, P.; Emelianova, E. V.; Bäessler, H., *Phys. Rev. B*, **2005**, *71*.
DOI: [10.1103/PhysRevB.71.045214](https://doi.org/10.1103/PhysRevB.71.045214)



A Monthly Journal

Advanced Materials Letters

Editor in Chief
Ashutosh Tiwari

Official journal of International Association of Advanced Materials
www.iaamonline.org

Copyright © 2016 VBRI Press AB, Sweden

Publish your article in this journal

VBRI Press
Commitment to Excellence

Advanced Materials Letters is an official international journal of International Association of Advanced Materials (IAAM, www.iaamonline.org) published monthly by VBRI Press AB from Sweden. The journal is intended to provide high-quality peer-review articles in the fascinating field of materials science and technology particularly in the area of structure, synthesis and processing, characterisation, advanced-state properties and applications of materials. All published articles are indexed in various databases and are available download for free. The manuscript management system is completely electronic and has fast and fair peer-review process. The journal includes review article, research article, notes, letter to editor and short communications.

www.vbripress.com/aml